Conventional Transmission Electron Microscopy Imaging beyond the Diffraction and Information Limits

Andreas Rosenauer,* Florian F. Krause, Knut Müller, Marco Schowalter, and Thorsten Mehrtens
Institute of Solid State Physics, University of Bremen, Otto-Hahn-Allee 1, 28359 Bremen, Germany
(Received 28 March 2014; revised manuscript received 17 July 2014; published 29 August 2014)

There are mainly two complementary imaging modes in transmission electron microscopy (TEM): Conventional TEM (CTEM) and scanning TEM (STEM). In the CTEM mode the specimen is illuminated with a plane electron wave, and the direct image formed by the objective lens is recorded in the image plane. STEM is based on scanning the specimen surface with a focused electron beam and collecting scattered electrons with an extended disk or ring-shaped detector. Here we show that combination of CTEM imaging with STEM illumination generally allows extending the point resolution of CTEM imaging beyond the diffraction limit. This new imaging mode improves imaging characteristics, is more robust against chromatic aberration, exhibits direct structural imaging with superior precision, visualizes light elements with excellent contrast, and even allows us to overcome the conventional information limit of a microscope.

DOI: 10.1103/PhysRevLett.113.096101 PACS numbers: 68.37.Og, 68.37.Ma

Introduction.—Since the end of the last millennium, transmission electron microscopy (TEM) has been improved dramatically by correctors for spherical [1–3] and chromatic aberration [4], which can be combined with a monochromated illumination system [5], pushing the information limit into the sub-Ångström range. The spatial resolution in the conventional TEM (CTEM) mode is determined by the maximum spatial frequency of the electron wave transferred by the optical system, termed the "diffraction limit." As the incoherent transfer function of a diffraction-limited system extends to twice the cutoff frequency of the coherent transfer function, it is expected that incoherent illumination leads to higher resolution. STEM imaging can be considered incoherent due to the principle of reciprocity [6], saying that it is equal to using a large incoherent illuminating source in CTEM [7,8]. Based on this idea, it was shown by Pennycook and Jesson [9] that annular dark-field (ADF) imaging provides direct structure images at atomic resolution. As furthermore shown by Nellist and Rhodenburg [10], chromatic aberration sets a fundamental information limit to the resolution of CTEM. Here, Nellist, McCalium and Rhodenburg [11] published resolution beyond this information limit by incoherent imaging realized by scanning TEM (STEM). Later, Nellist and Pennycook [12] demonstrated that incoherent TEM imaging is very robust to the effects of chromatic aberration and Kisielowki *et al.* [13] resolved atomic columns with 63 pm distance in ADF STEM. STEM imaging is therefore advantageous concerning resolution.

On the other hand, Van Aert and Van Dyck [14] pointed out that the precision for measurement of distances between atom columns depends on the number of electrons contributing to the image. This has an unfavorable effect for ADF STEM at specimen thicknesses below a few tens of nanometers, where only a small fraction of incident electrons hits the detector, resulting in a low signal-to-noise ratio. Another disadvantage of STEM imaging is the limited precision of positioning the electron probe, which leads to scan noise [15] reducing the precision at which atomic positions can be measured. Finally, the finite source size of the demagnified STEM emitter strongly affects spatial resolution. Verbeeck, Béché, and Van den Broek [16] measured the source profile with a holographic method and found its center dominated by a Gaussian part with a full width at half maximum of 0.1 to 0.2 nm, setting an information limit to STEM. As noted by Nellist and Pennycook [12], this limit can be improved by further demagnifying the source, but at the expense of the signal-to-noise ratio, which will itself provide a limit to the reachable precision. For CTEM, however, there is no scanning process and the source size is not the limiting factor, making CTEM superior in this manner. However, compared to STEM, the alignment of the correct focus is more difficult in CTEM as images show strong contrast and similar image patterns for large and small defoci. For the same reason, interpretation of CTEM images is not as straightforward as for STEM, where positions of atomic columns are easily identified.

Incoherent imaging can be realized in light optics using a self-luminous object, where different points of the specimen emit mutually incoherent light. This situation can be mimicked in CTEM imaging as illustrated in Fig. 1: The specimen is illuminated with a scanning, medium-resolution convergent electron beam. For each scan point an image is formed by the objective lens, and these images are summed up over one full area scan on a recording system such as a charge-coupled device (CCD) camera. This TEM mode thus combines STEM illumination with CTEM imaging and will be termed "imaging STEM" (ISTEM).

In the following, it is first demonstrated by simulation that ISTEM in fact allows imaging beyond the diffraction

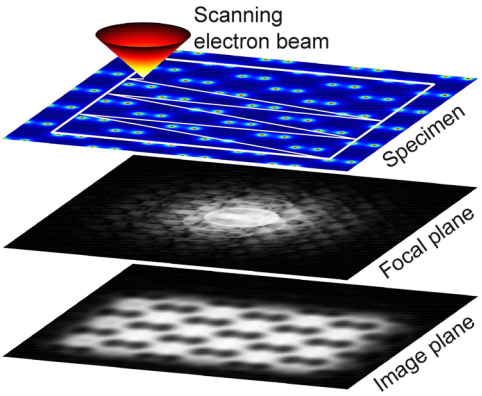

FIG. 1 (color online). The principle of the suggested imaging mode. The incoherence is obtained by scanning a focused electron probe over the specimen. For each probe position, the diffraction pattern in the focal plane of the objective lens shows diffraction discs. The recording system in the image plane acquires one image per complete area scan and, thus, integrates over all individual images, each of which corresponds to one position of the incident electron probe.

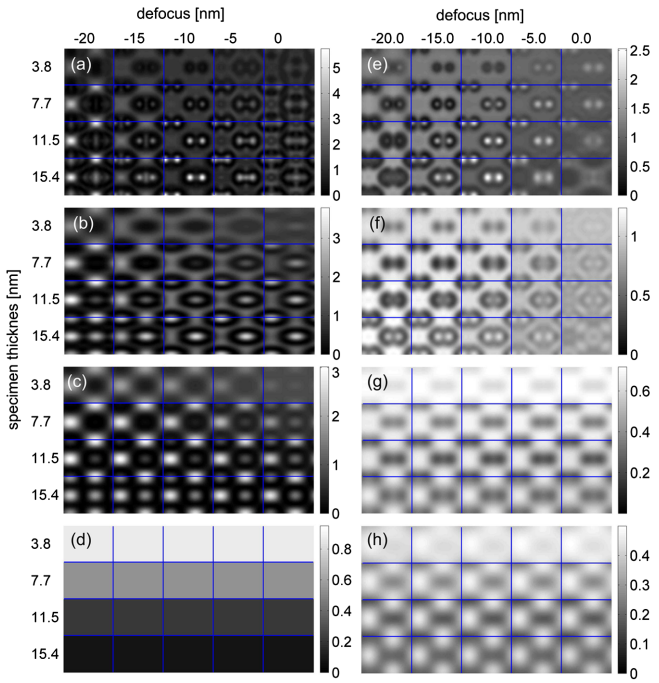

FIG. 2 (color online). Comparison of CTEM [(a) to (d)] and ISTEM [(e) to (h)] images simulated for a Si unit cell viewed along the [110] direction as a function of imaging system defocus and specimen thickness. The radius of the objective aperture corresponds to a diffraction limited resolution of (a) and (e) 55 pm, (b) and (f) 0.17 nm, (c) and (g) 0.27 nm, and (d) and (h) 0.33 nm, the spherical aberration of the imaging lens was $C_S = 50$ μm, and its defocus spread $\Delta = 3$ nm. For smaller objective apertures, the higher resolution of ISTEM imaging becomes apparent. While for CTEM the dumbbells are only visible in (a), they are still well resolved in (f) and even still faintly visible in (g).

limit and is more robust against chromatic aberration than CTEM, thus allowing imaging beyond the conventional information limit. Second, a theoretical description explaining why ISTEM images are almost independent of aberrations and defocus of the probe forming system is given and a further comparison to other imaging modes is drawn, revealing more advantages. Third, an ISTEM experiment that resolves details beyond the conventional information limit of the microscope is presented. Finally, we demonstrate improved precision of structure determination for ISTEM compared to STEM modes.

Imaging beyond the diffraction limit.—Figure 2 compares CTEM and ISTEM images for Si in [110] projection. The spherical aberration of the image forming lens was $C_S = 50$ μm, typical for aberration-corrected CTEM. Other simulation parameters are listed in the Supplemental Material S5 [17]. With the exception of the illumination, opposing ISTEM and CTEM images are computed for identical imaging conditions. In Figs. 2(b) to 2(d), the Si dumbbells cannot be resolved as their distance of 0.136 nm is beyond the diffraction limit defined by the radius of the objective aperture. The ISTEM image Fig. 2(f), however, clearly resolves the Si dumbbells, and they are even still faintly visible in Fig. 2(g), where the diffraction limited resolution is almost twice the dumbbell distance. In the bottommost row of Fig. 2 the objective aperture only contains the central beam, resulting in vanishing contrast in the CTEM image [Fig. 2(d)], whereas the lattice structure is still resolved in the ISTEM case except for the dumbbells as their atomic distance is smaller than half the diffraction limited resolution [Fig. 2(h)].

Imaging beyond the information limit.—Figure 3 displays the effect of the defocus spread associated with chromatic aberration on images obtained in CTEM and ISTEM mode, respectively. We assumed an aberration-free imaging lens and negligible semiconvergence angle of 0.002 mrad for the CTEM mode and simulated imaging of a diamond crystal with a dumbbell distance of 89 pm. The objective aperture had a radius equivalent to 20 pm; hence, this distance is not affected by the diffraction limit. Here, another benefit of the ISTEM mode is observed: Figs. 3(a) and 3(f) compare CTEM and ISTEM images for 0.2 nm imaging defocus spread, showing comparable intensity patterns and contrast. Figures 3(b) to 3(e) depict CTEM images for higher defocus spreads between $\Delta = 3$ and 24 nm, in comparison with ISTEM micrographs in Figs. 3(g) to 3(j). These images clearly reveal the different dependencies of CTEM and ISTEM imaging on the defocus spread, which as aforementioned is the prime origin of the CTEM information limit. Whereas in CTEM the dumbbells are hardly resolved already at a spread of $\Delta = 3$ nm [see Fig. 3(b)], which is a realistic value for a TITAN 80-300 G1 microscope [24], the dumbbells are clearly visible in all ISTEM images though beyond the information limits in Figs. 3(h) to 3(j). Figures 3(g) to 3(j) show that the intensity

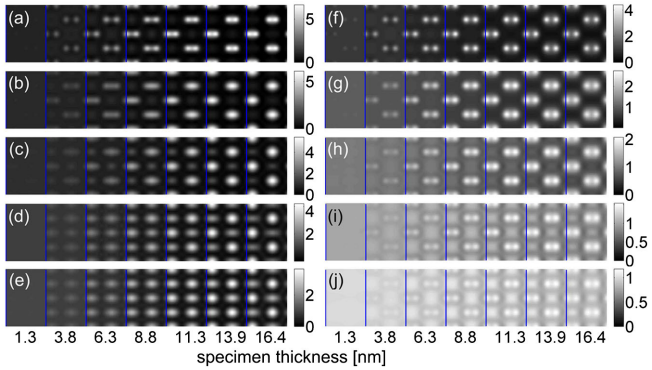

FIG. 3 (color online). Simulated images of a diamond crystal viewed along [110]: (a) to (e) CTEM images simulated with defocus spreads and corresponding information limits given in brackets of (a) 0.2 (20 pm), (b) 3 (81 pm), (c) 6 (0.11 nm), (d) 12 (0.16 nm), and (e) 24 nm (0.23 nm). (f) to (j) depict the corresponding ISTEM images, which clearly suffer less from the defocus spread as dumbbells are resolved even for (j) while for CTEM they are not resolved in (c) to (d).

patterns are similar for defocus spreads between 3 and 24 nm. The gray scale legends reveal decreasing contrast with increasing defocus spread in the case of ISTEM. The degradation of contrast admittedly also diminishes the precision with which the positions of the atom columns can be measured, and thus limits the resolution as defined in [14]. The decreased signal-to noise ratio can, however, be compensated for in the experiment by a larger dose, whereas a loss of resolution as shown in Fig. 3(e) cannot be compensated for by experimental conditions.

Comparison of imaging modes.—In the Supplemental Material S2 [17] it is rigorously shown that the mutual intensity of the ISTEM illumination is fully equivalent to the mutual intensity for CTEM imaging using a wide circular electron source, whose radius R_P in units of mrad is equal to the radius of the aperture in the probe-forming optics in the case of ISTEM. Applying the principle of reciprocity [6,7,25–27], this in turn means that in the case of a circular aperture ISTEM imaging is equivalent to STEM imaging with a bright-field (BF) detector whose radius in units of mrad is equal to R_P, if the ISTEM imaging lens and STEM probe forming lens exhibit identical aberrations. A resulting advantage of ISTEM, which it has in common with STEM, is vanishing image contrast for large defoci. This is demonstrated in the Supplemental Material S1 [17] in comparison with CTEM, where similar contrast patterns are observed for large and small defoci.

Nevertheless, there are important differences between BF STEM and ISTEM. In the former case, the width of the probe forming source leads to a decrease of image resolution, as two different points on the emitter correspond to two probes on the specimen surface shifted with respect to each other. In ISTEM the images for all probe positions are integrated; hence, source size has no influence on the image resolution. In addition, scan noise errors are circumvented in the ISTEM mode for the same reason. ISTEM therefore combines advantages of STEM, particularly the improved resolution of incoherent imaging, with direct imaging in the CTEM mode, while on the other hand, disadvantages of both modes are eliminated.

Another outcome of the calculation in the Supplemental Material S2 [17] is the mutual intensity of the ISTEM illumination being entirely independent of aberrations of the probe forming system. Thus, not only is probe correction not required, but also exact focusing of the probe on the specimen entrance plane is not important, only the scanned area might need to be increased accordingly, if the illuminating probe is broadened by aberrations. As to the aberrations of the imaging system, the Supplemental Material S3 [17] makes clear that they still have an important influence, making an image corrector advantageous for ISTEM.

A further advantage of ISTEM occurs for specimen drift, which results in a blurring of CTEM images damping higher image frequencies, but only leads to a distortion of the micrograph in ISTEM, which can be corrected afterwards [15].

Experimental resolution beyond the conventional information limit.—Figure 4 presents experimental ISTEM images of GaN taken on an image corrected microscope with a conventional information limit of 80 pm [28,29]. The specimen thickness was 8 to 12 nm determined by quantitative ADF STEM [30]. The thickness variation causes slight pattern changes over the images. Figure 4(a) was acquired in $[11\bar{2}0]$ projection; the Ga-N dumbbells with distance of 0.11 nm are very clearly resolved as shown in the magnified area. While this distance is within the information limit, it is remarkable that the columns of the light N atoms are clearly visible, which could be achieved by neither CTEM nor ADF STEM. As Fig. 4(b) shows, the observed patterns are in good agreement with simulations for different defoci, validating the simulation results. Figure 4(c) displays a $[1\bar{1}00]$ projection, where the Ga-N distance is only 63 pm—significantly beyond the conventional information limit of our microscope. The dumbbells are, however, recognizably resolved. The according diffractogram [Fig. 4(d)] also spreads out to frequencies related to this distance. The advantageous properties of ISTEM evidently allow to push a microscope's CTEM information limit significantly further without any modification to the hardware.

Superior precision of direct structure evaluation.—To investigate the precision of direct structure evaluation using ISTEM, we simulated imaging of a pseudomorphic $In_xGa_{1-x}As/GaAs$ heterostructure. The In concentration x gradually increases to 30% causing a 4% change in lattice plane distance. Probe-corrected ADF STEM with a 36–300 mrad detector, BF STEM (0–21 mrad), and image corrected ISTEM images were computed. Shot noise was applied to all three images. We assumed an electron beam with 9 mrad semiconvergence angle and a dose of 300 electrons per pixel for ISTEM, whereas the dose was

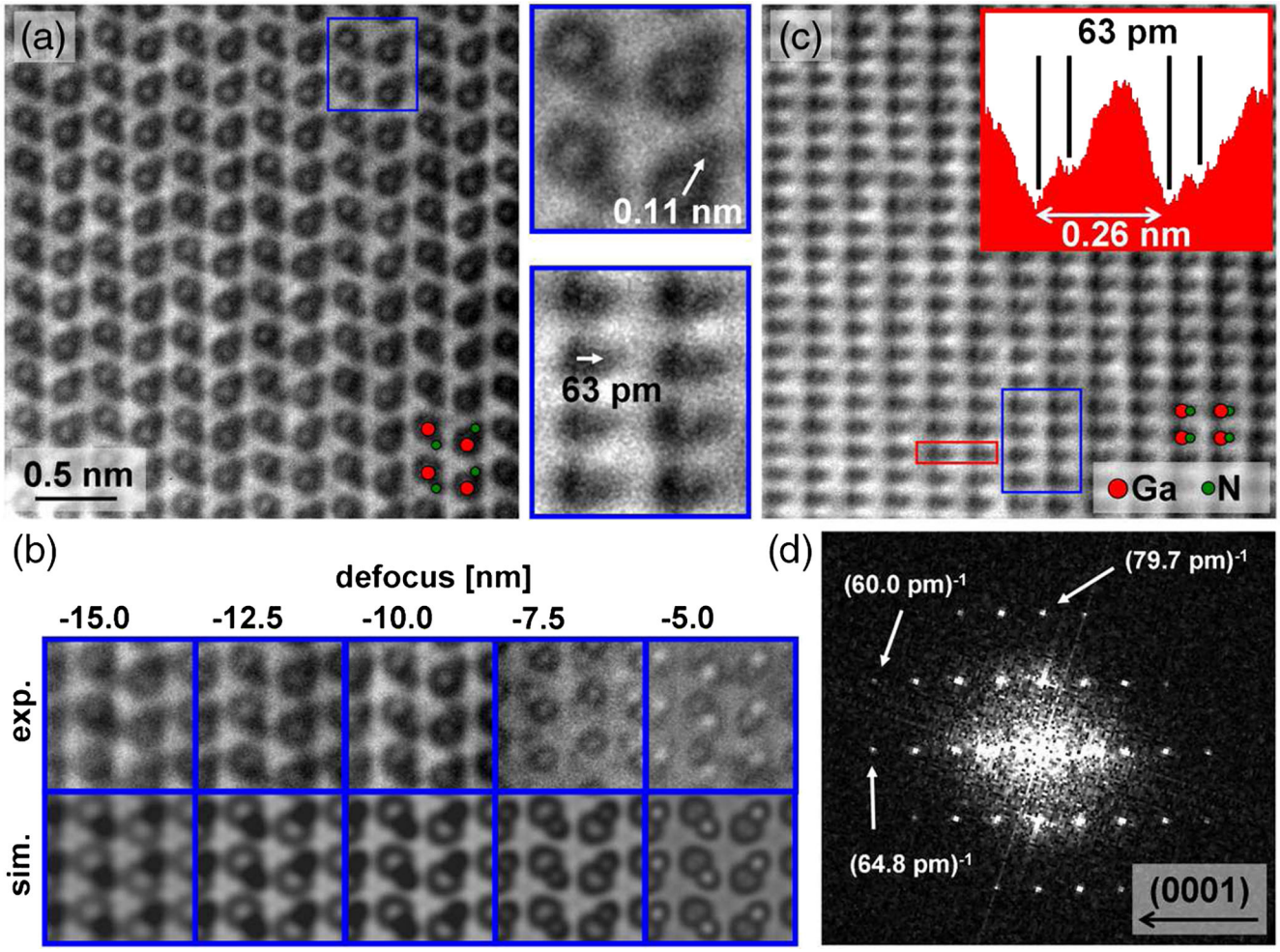

FIG. 4 (color online). Experimental ISTEM micrographs of GaN of about 10 nm thickness. (a) Acquired in [11$\bar{2}$0] projection. (b) The comparison of a defocus series with simulation from the same orientation. (c) A [1$\bar{1}$00] projection. The line scan in the inset corresponds to the area marked in red. (d) Diffractogram of (c). The central insets show magnifications of (a) and (b) taken from the regions marked in blue, respectively. The Ga-N dumbbells are well resolved even in (c), where the distance of 63 pm is beyond the information limit.

increased to 1630 electrons per pixel for the STEM imaging modes accounting for the 21 mrad condenser aperture. For STEM imaging, the broadening of the probe due to the finite source size with 80 pm full width at half maximum and scan noise with root-mean squared probe displacements of 20 pm were simulated. Both values underestimate typical experimental conditions following Refs. [16] and [15]. As described above, ISTEM is affected by neither.

These images were evaluated by fitting a Gaussian based parametric model to each atomic column as described in [31]. From the positions of the atom columns we calculated the lattice strain. Figures 5(a) to 5(c) show the simulated micrographs and the respective fitted models, while Fig. 5(d) depicts the resulting strain profiles. The evaluation of the ISTEM image well resembles the true profile and the error bars are significantly smaller than those corresponding to BF STEM and ADF STEM, clearly revealing the improvement of precision by ISTEM. We found that this also holds for BF simulations without scan noise.

Fields of application.—ISTEM has a large field of promising applications. It can be used in modern electron microscopes that are able to combine STEM illumination with CTEM imaging, thereby improving spatial resolution as well as interpretability of structure images. It provides imaging characteristics typical for aberration-corrected STEM for aberration-corrected CTEM imaging. Thanks to reciprocity, ISTEM is capable of applying techniques, which currently require aberration-corrected STEM, in aberration-corrected CTEM. One example is annular-bright field (ABF) imaging [8,32], which plays an important role for imaging of the lightest elements in the vicinity of heavier elements. It requires a ring detector, which in the case of ISTEM is equivalent to a ring-shaped aperture in the probe forming system as shown in the Supplemental Material S4 [17]. The CTEM equivalent of ABF due to reciprocity [8] is hollow-cone illumination (HCI) [33–36], providing an improvement of resolution using a ring-shaped source. An extended source, however, is not easily

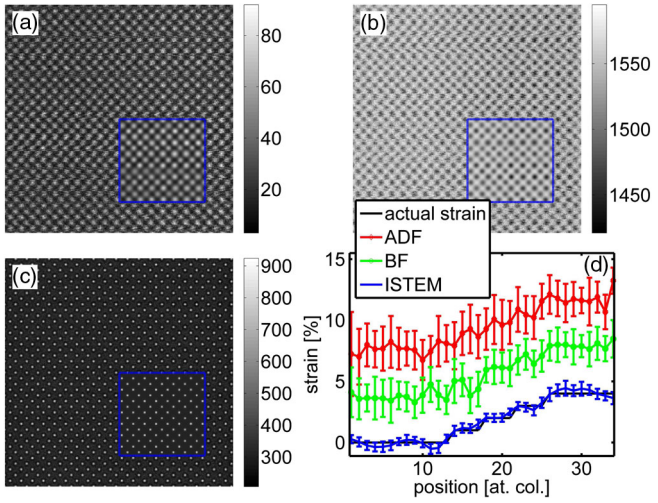

FIG. 5 (color online). (a)–(c) Simulated images of a GaAs/InGaAs interface viewed in [100] projection with a strain gradient from 0% to 4% from left to right corresponding to the [001] direction. The blue framed insets show the fitted parametric model. Imaging mode: (a) ADF, (b) BF and (c) ISTEM. The legends are given in units of "number of electrons". (d) shows the strain profiles resulting from each fit, where the curves from BF and ADF are shifted upwards by 4% and 8%, respectively. The precision for ISTEM is more than twice as good as for the scanning methods. The error bars are retrieved from the standard deviation in averaging direction.

realized in modern microscopes that are optimized for high spatial coherence, and connected with problems such as nonisoplanatism and inhomogeneous illumination. In ISTEM HCI-like imaging becomes easily applicable with annular probe forming apertures and would benefit from reduced specimen drift sensitivity.

Application of ISTEM allowed us to image light nitrogen atomic columns close to much heavier Ga columns [Fig. 4(a)] and to resolve distances below 80 pm [Fig. 4(c)], which on our microscope would not have been possible otherwise. Thus, it is conceivable that ISTEM likewise allows pushing the point resolution of more advanced microscopes even below 50 pm. Because of its ability to combine advantages of STEM and CTEM while avoiding drawbacks of both, we expect ISTEM to become an important imaging mode in the near future.

This work was supported by the Deutsche Forschungsgemeinschaft under Contract No. RO 2057/8-1. A. R. and F. K. contributed equally to this work and thus share first-authorship.

*rosenauer@ifp.uni-bremen.de

[1] P. E. Batson, N. Dellby, and O. L. Krivanek, Nature (London) **418**, 617 (2002).
[2] S. Uhlemann and M. Haider, Ultramicroscopy **72**, 109 (1998).
[3] M. Haider, S. Uhlemann, E. Schwan, H. Rose, B. Kabius, and K. Urban, Nature (London) **392**, 768 (1998).
[4] M. Haider, P. Hartel, H. Müller, S. Uhlemann, and J. Zach, Microsc. Microanal. **16**, 393 (2010).
[5] B. Freitag, S. Kujawa, P. M. Mul, J. Ringnalda, and P. C. Tiemeijer, Ultramicroscopy **102**, 209 (2005).
[6] A. P. Pogany and P. S. Turner, Acta Crystallogr. Sect. A **24**, 103 (1968).
[7] J. M. Cowley, Appl. Phys. Lett. **15**, 58 (1969).
[8] R. Ishikawa, E. Okunishi, H. Sawada, Y. Kondo, F. Hosokawa, and E. Abe, Nat. Mater. **10**, 278 (2011).
[9] S. J. Pennycook and D. E. Jesson, Phys. Rev. Lett. **64**, 938 (1990).
[10] P. D. Nellist and J. M. Rodenburg, Ultramicroscopy **54**, 61 (1994)
[11] P. D. Nellist, B. C. McCalium, and J. M. Rodenburg, Nature (London) **374**, 630 (1995).
[12] P. D. Nellist and S. J. Pennycook, Phys. Rev. Lett. **81**, 4156 (1998).
[13] C. Kisielowski *et al.*, Microsc. Microanal. **14**, 469 (2008).
[14] S. Van Aert and D. Van Dyck, Opt. Express **14**, 3830 (2006).
[15] L. Jones and P. D. Nellist, Microsc. Microanal. **19**, 1050 (2013).
[16] J. Verbeeck, A. Béché, and W. Van den Broek, Ultramicroscopy **120**, 35 (2012).
[17] See Supplemental Material at http://link.aps.org/supplemental/10.1103/PhysRevLett.113.096101, which includes Refs. [18–23].
[18] M. Haider, H. Rose, S. Uhlemann, E. Schwa, B. Kabius, and K. Urban, Ultramicroscopy **75**, 53 (1998).
[19] J. Verbeeck, D. Van Dyck, H. Lichte, P. Potapov, and P. Schattschneider, Ultramicroscopy **102**, 239 (2005).
[20] J. Frank, Optik (Stuttgart) **38**, 171 (1969).
[21] A. Rosenauer and M. Schowalter, *Springer Proceedings in Physics* (Springer, Netherlands, 2008), Vol. 120, p. 169.
[22] D. Van Dyck, Ultramicroscopy **111**, 894 (2011).
[23] F. F. Krause, K. Müller, D. Zillmann, J. Jansen, M. Schowalter, and A. Rosenauer, Ultramicroscopy **134**, 94 (2013).
[24] P. C. Tiemeijer, *Titan Condenser Manual* (FEI Company, Eindhoven, 2005).
[25] M. von Laue, Materiewellen und ihre Interferenzen, Leipzig 1948.
[26] R. J. Potton, Rep. Prog. Phys. **67**, 717 (2004).
[27] D. E. Bilhorn, L. L. Foldy, R. M. Thaler, W. Tobocman, and V. A. Madsen, J. Math. Phys. (N.Y.) **5**, 435 (1964).
[28] *FEI Production Management*, Titan Series Certificate of Instrument Quality (FEI Company, Eindhoven, 2005).
[29] J. Barthel and A. Thust, Phys. Rev. Lett. **101**, 200801 (2008).
[30] A. Rosenauer *et al.*, Ultramicroscopy **111**, 1316 (2011).
[31] A. J. den Dekker, J. Gonnissen, A. De Backer, J. Sijbers, and S. Van Aert, Ultramicroscopy **134**, 34 (2013).
[32] S. D. Findlay, N. Shibata, H. Sawada, E. Okunishi, Y. Kondo, and Y. Ikuhara, Ultramicroscopy **110**, 903 (2010).
[33] K. Hanszen and L. Trepte, Optik (Stuttgart) **33**, 166 (1971).
[34] H. Rose, Ultramicroscopy **2**, 251 (1977).
[35] C. Dinges, H. Kohl, and H. Rose, Ultramicroscopy **55**, 91 (1994).
[36] W. Kunath, F. Zemlin, and K. Weiss, Ultramicroscopy **16**, 123 (1985).